JACS Au
AN OPEN ACCESS JOURNAL OF THE AMERICAN CHEMICAL SOCIETY

Editors' Choice
Open Access

pubs.acs.org/jacsau
Article

Relay Catalysis for Highly Selective Conversion of Methanol to Ethylene in Syngas

Kuo Chen, Fenfang Wang, Yu Wang, Fuyong Zhang, Xinyu Huang, Jincan Kang,* Qinghong Zhang,* and Ye Wang*

Cite This: JACS Au 2023, 3, 2894−2904
Read Online

ACCESS | Metrics & More | Article Recommendations | Supporting Information

ABSTRACT: The precise C−C coupling is a challenging goal in C1 chemistry. The conversion of methanol, a cheap and easily available C1 feedstock, into value-added and largely demanded olefins has been playing a game-changing role in the production of olefins. The current methanol-to-olefin (MTO) process, however, suffers from limited selectivity to a specific olefin. Here, we present a relay-catalysis route for the high-selective conversion of methanol to ethylene in syngas (H_2/CO) typically used for methanol synthesis. A bifunctional catalyst composed of selectively dealuminated H-MOR zeolite and ZnO−TiO_2, which implemented methanol carbonylation with CO to acetic acid and selective acetic acid hydrogenation to ethylene in tandem, offered ethylene selectivity of 85% at complete methanol conversion at 583 K. The selective removal of Brønsted acid sites in the 12-membered ring channel of H-MOR favors the selectivity of acetic acid in CH_3OH carbonylation. The high capabilities of ZnO−TiO_2 in the adsorption of acetic acid and the activation of H_2 play key roles in selective hydrogenation of acetic acid to ethylene. Our work provides a promising relay-catalysis strategy for precise C−C coupling of C1 to C2 molecules.

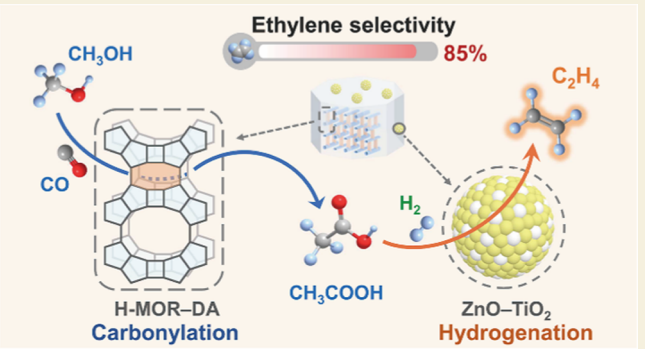

KEYWORDS: *C1 chemistry, relay catalysis, ethylene, methanol carbonylation, C−C coupling*

INTRODUCTION

As an abundant and cheap C1 feedstock, methanol can be derived not only from various carbon resources, such as natural or shale gas, coal, and biomass via syngas (H_2/CO), but also from CO_2 and renewable solar energy via the "liquid sunshine" strategy.[1,2] The significance of methanol as a key platform for the supply of energy and chemicals has long been recognized and will become more important under the background of carbon neutrality aiming to recycle carbon dioxide with renewable energy into carbon feedstocks.[3] The utilization of methanol to replace crude oil for the production of largely demanded building-block chemicals in the chemical industry is a highly attractive research direction. As a representative example, the methanol-to-olefin (MTO) process has contributed to broadening the olefin feedstock and has received wide attention from both academic and industrial communities.[4−8]

Among various olefins, ethylene, which is widely used for the manufacture of plastics, fibers, and other high-value chemicals, is the largest demanded building block in the current chemical industry with annual production of >150 million tons.[9] Besides the cracking of naphtha, the synthesis of C_2H_4 from C1 feedstocks such as CH_3OH, syngas, or even CO_2 has also attracted much recent attention.[4,5,10−13] The syngas or CO_2-based olefin synthesis typically proceeds via the following three routes: (1) the modified Fischer−Tropsch (FT) synthesis route (Scheme 1, Route A), (2) the direct conversion route with bifunctional metal oxide−zeolite catalysts via methanol or ketene intermediate (Scheme 1, Route B), and (3) the indirect route via two processes of methanol synthesis and MTO (Scheme 1, Route C).[10−13] The product selectivity of Route A is limited by the Anderson−Schulz−Flory (ASF) distribution with a maximum selectivity of C_{2-4} hydrocarbons (including both olefins and paraffins) of 58%,[10] while the product formation of Routes B and C is typically controlled by the shape selectivity of zeolites.[4,5,11,12] The selectivity of C_2−C_4 olefins ($C_{2-4}^{=}$) reaches ∼90% in the MTO reaction, but that of C_2H_4 is typically limited to ∼45% even after the engineering of the topology and the cage or cavity of small-pore zeolites.[14,15] Normally, a similar selectivity pattern of olefins has been obtained for Route B, although a couple of studies have

Received: August 10, 2023
Revised: September 26, 2023
Accepted: September 28, 2023
Published: October 15, 2023

Scheme 1. Potential Routes for Synthesis of Ethylene from C1 Feedstocks

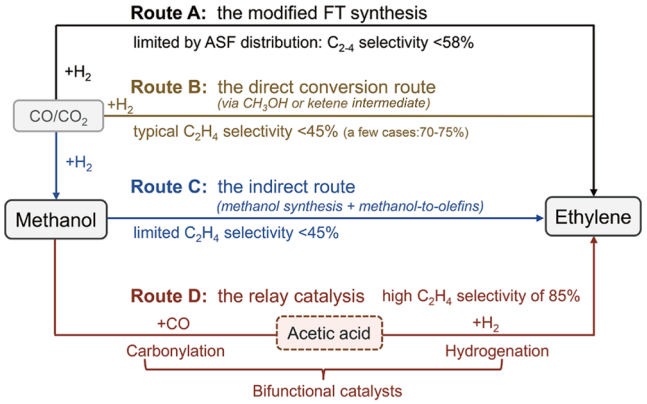

reported C_2H_4 selectivity of 70−75% from CO or CO_2 hydrogenation over bifunctional catalysts.[16,17] The development of new strategies is required to achieve the goal of synthesizing C_2H_4 with higher selectivity from C1 molecules.

The carbonylation of CH_3OH with CO to acetic acid (AA) is another important C1 chemical reaction involving C−C coupling. This reaction offers the sole C_2 compound and is thus more precise in C−C coupling than the MTO reaction that produces a C_{2-4} mixture. The CH_3OH carbonylation is conventionally catalyzed by a homogeneous Rh or Ir complex catalyst in the presence of an iodide promoter.[18] Heterogeneous catalytic carbonylation has made significant progress owing to the discovery of zeolite H-mordenite (H-MOR) for the carbonylation of dimethyl ether (DME) without the need of halide promoters.[19−21] Based on the H-MOR-catalyzed C−C coupling, we developed a strategy of relay catalysis for single-pass conversion of syngas into ethanol via a layer-by-layer configuration of three-stage catalysts, i.e., (1) syngas to DME/CH_3OH, (2) DME/CH_3OH carbonylation to methyl acetate (MA)/AA, and (3) hydrogenation of MA/AA to ethanol.[22,23] We found that the use of physical mixture of the three-stage catalysts instead of the layer-by-layer configuration offered C_2H_4 with a selectivity of about 65% at a CO conversion of 10%.[22] This encouraging result stimulates us to develop a more selective route for the synthesis of C_2H_4 from C1 feedstocks.

Here, we present a relay-catalysis route for the high-selective synthesis of C_2H_4 from CH_3OH in the presence of syngas (Scheme 1, Route D). Considering that CH_3OH is industrially produced from syngas and the single-pass conversion is usually controlled by the compromise between thermodynamics and

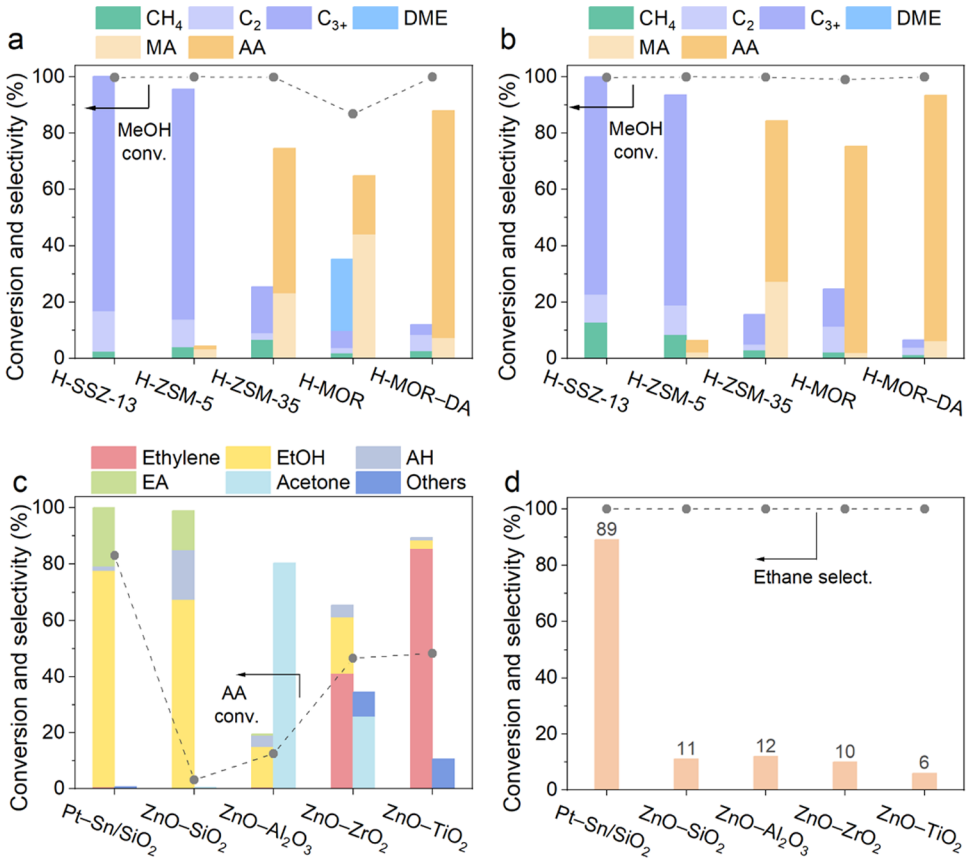

Figure 1. Catalytic behaviors of zeolites in methanol carbonylation and metal oxides in hydrogenation of acetic acid and ethylene. (a) Methanol carbonylation with CO over zeolites. C_2 and C_{3+} denote C_2 and C_{3+} hydrocarbons, respectively. (b) Methanol carbonylation in syngas over zeolites. (c) Hydrogenation of acetic acid over metal oxides as well as Pt−Sn/SiO_2. AH and EA denote acetaldehyde and ethyl acetate, respectively. Others include CH_4, C_2 paraffins, and C_{3+} hydrocarbons. (d) Hydrogenation of ethylene over metal oxides as well as Pt−Sn/SiO_2. No CO_2 was detected in all of the cases. Reaction conditions for panels (a) and (b): zeolite, 0.33 g; T = 583 K; P = 3 MPa; F(CH_3OH vapor) = 0.70 mL min^{-1}; time on stream, 5 h; F(N_2/CO) = 90 mL min^{-1} and N_2/CO = 1 for panel (a); and F(H_2/CO) = 90 mL min^{-1} and H_2/CO = 1 for panel (b). Reaction conditions for panels (c) and (d): catalyst, 0.66 g; T = 583 K; P = 3 MPa; F(total) = 90 mL min^{-1}; H_2/AA = 48/1 for panel (c); and H_2/C_2H_4 = 89/1 for panel (d).

https://doi.org/10.1021/jacsau.3c00463
JACS Au 2023, 3, 2894−2904

kinetics, the conversion of CH_3OH in the presence of syngas to C_2H_4 would provide an alternative to the MTO process for C_2H_4 synthesis. Our idea is to integrate a catalyst for CH_3OH carbonylation with CO in syngas and a catalyst for AA hydrogenation to C_2H_4. Through the development of a bifunctional catalyst composed of modified H-MOR and a binary metal oxide, we achieve 85% selectivity of C_2H_4 at nearly 100% CH_3OH conversion.

RESULTS AND DISCUSSION

Catalysts for Methanol Carbonylation and Acetic Acid Hydrogenation

To construct an efficient bifunctional catalyst for the transformation of CH_3OH to C_2H_4, we first studied potential catalysts for the carbonylation of CH_3OH with CO, i.e., the first step of the relay catalysis. In spite of significant advances in the carbonylation of DME using H-MOR, studies on non-noble-metal-based CH_3OH carbonylation catalysts are still very limited.[24,25] We found that the conversion of CH_3OH was almost 100% over some typical zeolites at 583 K, but the product distribution depended significantly on the zeolite (Figure 1a). While H-SSZ-13 and H-ZSM-5 mainly offered C_{2+} hydrocarbons (including olefins and paraffins), C_2 oxygenates (including AA and MA) were the major products over H-ZSM-35 and H-MOR. Considering that the latter two zeolites contain eight-membered ring (8-MR) channels, this result agrees well with the insight obtained from the carbonylation of DME that the Brønsted acid sites located in the 8-MR channel are capable of catalyzing carbonylation via the Koch-type reaction, i.e., the strong-acid-catalyzed insertion of CO into C−O bond of an alcohol and the subsequent conversion of the formed acetyl intermediate.[26] On the other hand, the Brønsted acid sites located in the 12-MR or 10-MR channel are responsible for the conversion of CH_3OH to hydrocarbons (i.e., the MTH reaction).[20,21] A high-temperature steam-treatment method was adopted for selective dealumination in the 12-MR channel of H-MOR.[21] Our characterizations showed that the crystalline structure and the morphology of the obtained H-MOR−DA catalyst did not change significantly (Figures S1 and S2). The ammonia temperature-programmed desorption (NH_3-TPD) and Fourier transform infrared (FT-IR) results confirmed that a large fraction of Brønsted acid sites in the 12-MR channel of H-MOR−DA was removed, while most of those in the 8-MR channel and the intersections between 8-MR and 12-MR channels were preserved (Figures S3 and S4, and Table S1). The selective dealumination significantly increased the selectivity of AA into 82% at the expense of that of MA and the total selectivity of (AA + MA) was 91%. This is probably because the presence of 12-MR channels also favors the formation of DME and its carbonylation gave MA. The result further emphasizes the importance of the Brønsted acid sites located in the 8-MR channel of H-MOR in CH_3OH carbonylation. In the absence of CO, hydrocarbons became the predominant products over all of the zeolites including H-MOR and H-MOR−DA (Figure S5), providing further evidence that AA and MA are formed via the carbonylation reaction with CO. It is noteworthy that the copresence of H_2 with CO changed the product selectivity to some extent. The selectivity of (AA + MA) was enhanced over H-ZSM-35, H-MOR, and H-MOR−DA (Figure 1b). The enhancing effect of H_2 was once reported in the H-MOR-catalyzed DME carbonylation to MA probably owing to the suppression of the deactivation by coke deposition.[27] The selectivity values of AA and (AA + MA) over H-MOR−DA were enhanced to 85% and 94%, respectively (Figure 1b). Further, no significant deactivation of H-MOR−DA was observed for CH_3OH carbonylation in syngas in 50 h of reaction (Figure S6). The favorable effect of copresence of H_2 on carbonylation is beneficial to the present relay-catalysis route.

Then, we studied the potential catalysts for the hydrogenation of AA to C_2H_4, i.e., the second step of our relay catalysis. Supported Pt−Sn catalysts were known to be capable of catalyzing the hydrogenation of AA to ethanol under conditions matching with those used for CH_3OH carbonylation.[23] Our present work confirmed that the Pt−Sn/SiO_2 catalyst was efficient for AA hydrogenation, providing ethanol with selectivity of about 80% at an AA conversion of 83% at 583 K (Figure 1c). Considering that ethanol may undergo facile dehydration to C_2H_4 over the bifunctional catalyst containing a zeolite, we combined the Pt−Sn/SiO_2 catalyst and the zeolite employed in the first step by physical mixing for CH_3OH conversion in syngas. Hydrocarbons with broad distributions were formed over the bifunctional catalyst containing zeolite H-SSZ-13 or H-ZSM-5, whereas the selectivity of C_2 hydrocarbons was significantly higher over that containing zeolite H-ZSM-35, H-MOR, or H-MOR−DA (Figure S7), in agreement with fact that these zeolites could catalyze the precise C−C coupling via CH_3OH carbonylation to AA. However, only the bifunctional catalyst composed of H-MOR−DA and Pt−Sn/SiO_2 prepared by physical mixing (denoted as H-MOR−DA+Pt−Sn/SiO_2) offered a considerable selectivity of C_2H_4 (55%) (Figure S7). C_2H_6 and C_{3+} hydrocarbons were formed as byproducts over the Pt−Sn/SiO_2-based bifunctional catalyst. Therefore, new catalysts should be developed for the hydrogenation of AA to improve the selectivity of C_2H_4.

We investigated a series of ZnO-based binary metal oxides for the hydrogenation of AA, considering their unique selectivity in hydrogenation of C═O bonds versus C═C bonds.[28−31] The typical ZnO content in the binary metal oxides was regulated to 10 wt %. While ZnO−SiO_2 and ZnO−Al_2O_3 were less active for AA hydrogenation, ZnO−ZrO_2 and ZnO−TiO_2 displayed significantly higher AA conversions at 583 K (Figure 1c). It is of interest that the major product depended significantly on the binary metal oxide. Ethanol was mainly formed over the ZnO−SiO_2 catalyst, while acetone became the major product over the ZnO−Al_2O_3 catalyst probably because of the occurrence of ketonization reaction.[32] C_2H_4 was formed as a major product over ZnO−ZrO_2 and ZnO−TiO_2, and in particular, the latter catalyst showed an excellent C_2H_4 selectivity of 83% (Figure 1c). This indicates that these binary metal oxides not only have an excellent hydrogenation/dehydration or hydrodeoxygenation ability but also may keep C_2H_4 from undergoing hydrogenation to C_2H_6. The control experiment reveals that the Pt−Sn/SiO_2 catalyst was highly active for the hydrogenation of C_2H_4 to C_2H_6, whereas the C_2H_4 hydrogenation proceeded negligibly over the binary metal oxides at 583 K (Figure 1d). Therefore, the present work demonstrates that ZnO−TiO_2 behaves quite differently from Pt−Sn/SiO_2 in the hydrogenation of AA, holding potential as a better component for C_2H_4 formation in the bifunctional catalyst.

https://doi.org/10.1021/jacsau.3c00463
JACS Au 2023, 3, 2894−2904

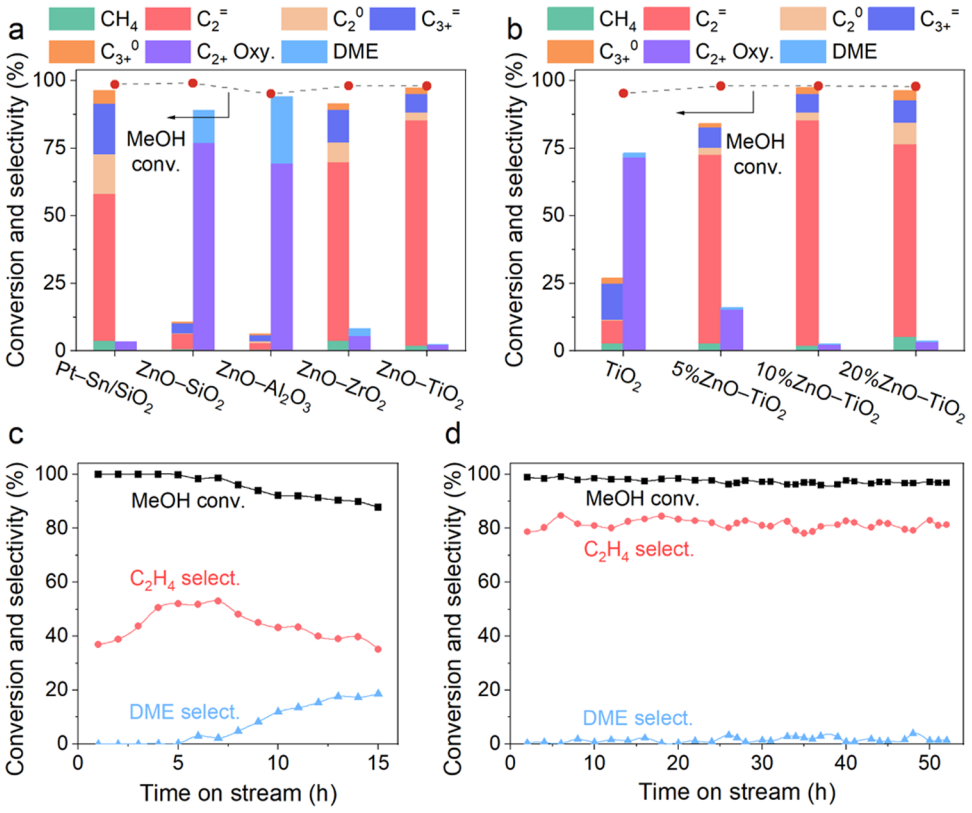

Figure 2. Catalytic behaviors of bifunctional catalysts for the conversion of CH_3OH in syngas. (a) Bifunctional catalysts of H-MOR−DA+different AA hydrogenation catalysts. $C_2^=$, C_2^0, $C_{3+}^=$, C_{3+}^0, and C_{2+} Oxy. denote C_2H_4, C_2H_6, C_{3+} olefins, C_{3+} paraffins, and C_{2+} oxygenates, respectively. C_{2+} Oxy. included AA, MA, ethyl acetate, and acetone. (b) Bifunctional catalysts of H-MOR−DA+ZnO−TiO_2 catalysts with different ZnO contents. (c) Stability of H-MOR−DA+Pt−Sn/SiO_2. (d) Stability of H-MOR−DA+ZnO−TiO_2. Reaction conditions: H-MOR−DA, 0.33 g; hydrogenation catalyst, 0.66 g; T = 583 K; P = 3 MPa; $F(CH_3OH$ vapor) = 0.7 mL min^{-1}; H_2/CO = 1; F(total) = 90 mL min^{-1}; and time on stream, 5 h for panels (a) and (b).

Bifunctional Catalysts for Methanol to Ethylene

Subsequently, we studied the bifunctional catalysts prepared by physical mixing of H-MOR−DA and different AA hydrogenation catalysts. C_{2+} oxygenates, mainly acetic acid, resulting from CH_3OH carbonylation were the major products over the H-MOR−DA+ZnO−SiO_2 and H-MOR−DA+ZnO−Al_2O_3 catalysts (Figure 2a). This is due to the low activities of ZnO−SiO_2 and ZnO−Al_2O_3 in the hydrogenation of AA. The presence of DME as a byproduct indicates the occurrence of methanol dehydration besides the methanol carbonylation over these catalysts. In contrast, the H-MOR−DA+ZnO−ZrO_2 and H-MOR−DA+ZnO−TiO_2 catalysts demonstrated a C_2H_4 selectivity of >60% at CH_3OH conversions of >95%, better than the H-MOR−DA+Pt−Sn/SiO_2 catalyst. As compared to the ZnO−ZrO_2-based bifunctional catalyst, the H-MOR−DA +ZnO−TiO_2 catalyst showed higher C_2H_4 selectivity. The H-MOR−DA+TiO_2 catalyst without ZnO only showed very low C_2H_4 selectivity and C_{2+} oxygenates remained as the major product (Figure 2b). The incorporation of 5.0 wt % ZnO into TiO_2 markedly shifts the major product to C_2H_4. The selectivity of C_2H_4 reached the maximum of 85% at a ZnO content of 10%. Therefore, ZnO plays a crucial role in the hydrogenation of AA to C_2H_4. A too higher content of ZnO (20 wt %) would cause overhydrogenation, decreasing the selectivity of C_2H_4 and increasing that of C_2H_6. As far as we know, the C_2H_4 selectivity of 85% is significantly higher than that reported in the MTO reaction (Table S2). Further, the C_2H_4 formation rate achieved by the present relay-catalysis route is comparable or at least not too lower as compared to the conventional MTO route (Table S2). Therefore, the present work offers a candidate of MTO for the highly selective synthesis of C_2H_4.

It is noteworthy that the bifunctional catalyst based on ZnO−TiO_2 is significantly more stable than that based on Pt−Sn/SiO_2 (Figure 2c,2d). Both the CH_3OH conversion and C_2H_4 selectivity underwent gradual decreases after about 7 h of reaction over the H-MOR−DA+Pt−Sn/SiO_2 catalyst (Figure 2c). The selectivity of DME increased gradually at the same time. This suggests that the catalyst deactivation arises from the decreased ability of zeolite in catalyzing CH_3OH carbonylation, leading to the dehydration of methanol to DME. In contrast, the H-MOR−DA+ZnO−TiO_2 catalyst displayed stable performance; both the CH_3OH conversion and the C_2H_4 selectivity did not undergo significant changes in 50 h of reaction (Figure 2d).

The presence of H_2O is detrimental to the H-MOR-catalyzed carbonylation of either DME or methanol.[19,25] Ni et al. reported an increase in the selectivity of DME at the expense of that of AA after the addition of H_2O into the CH_3OH feed over a pyridine-modified H-MOR catalyst.[25] We found that in the presence of syngas, the addition of H_2O to CH_3OH similarly reduced the selectivity of AA and increased that of MA and DME over the H-MOR−DA catalyst (Figure S8). We speculate that the excessive water formed during acetic acid hydrogenation can be adsorbed on the Brønsted acid site in the 8-MR channel of H-MOR−DA,[20,22,25] thus

https://doi.org/10.1021/jacsau.3c00463
JACS Au 2023, 3, 2894−2904

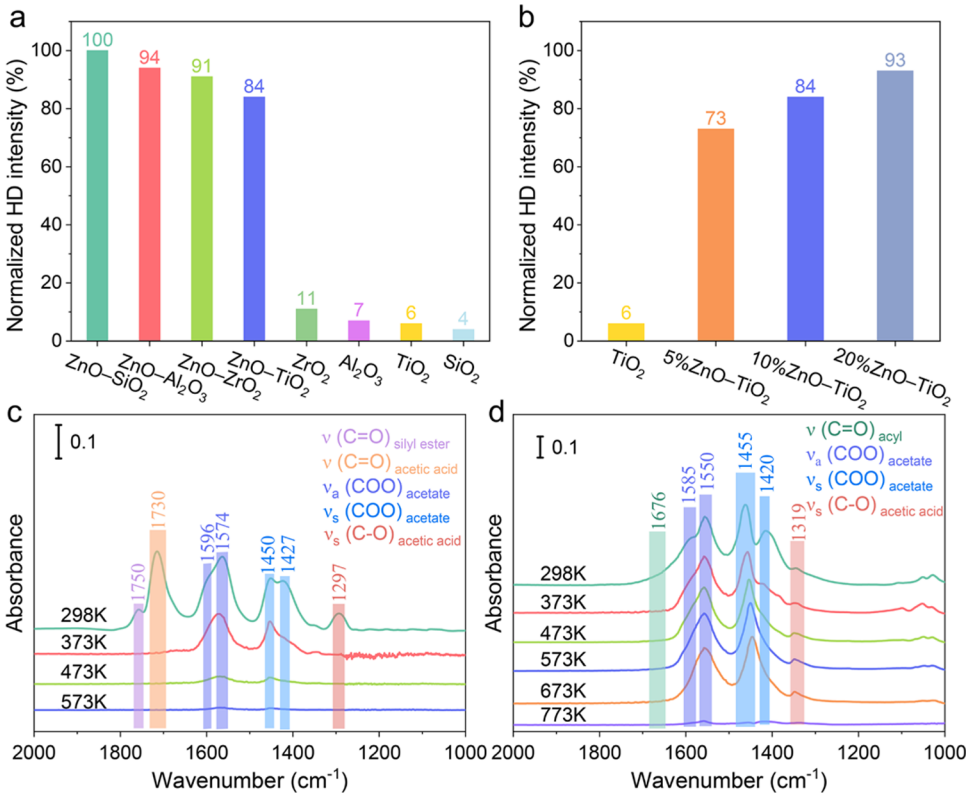

Figure 3. Normalized HD formation rate and FT-IR spectra of adsorbed acetic acid. (a) Normalized HD formation rate over different metal oxides. (b) Normalized HD formation rate over ZnO−TiO_2 catalysts with different ZnO contents. (c) FT-IR spectra of adsorbed acetic acid at varied temperatures on ZnO−SiO_2. (d) FT-IR spectra of adsorbed acetic acid at varied temperatures on ZnO−TiO_2.

suppressing the methanol carbonylation and leading to the side reactions of methanol to DME and hydrocarbons as well as the catalyst deactivation. In our relay-catalysis system, the hydrogenation of AA into C_2H_4 over Pt−Sn/SiO_2 or ZnO−TiO_2 would produce H_2O and the formed water may diffuse to the H-MOR−DA particle, thus exerting a negative effect on the stability of H-MOR−DA. We believe that this results in the deactivation of the H-MOR−DA+Pt−Sn/SiO_2 catalyst. It is thus of interest to unveil the reason why the H-MOR−DA +ZnO−TiO_2 catalyst can keep stable under such circumstance.

Considering the capability of ZnO-based metal oxides in catalyzing the water−gas shift (WGS) reaction ($CO + H_2O \rightarrow CO_2 + H_2$),[29,33] we speculate that the WGS reaction may take place between the formed H_2O and CO in syngas over ZnO−TiO_2. This may remove H_2O from the ZnO−TiO_2-based relay-catalytic system. Our studies confirmed that no conversion of CO or H_2O occurred without a catalyst, and both H-MOR−DA and Pt−Sn/SiO_2 were also inactive for the WGS reaction at 583 K. In contrast, the ZnO−TiO_2 catalyzed the WGS reaction efficiently and the conversion of H_2O reached 50% at a H_2O/CO ratio of 0.175 at 583 K (Table S3). We also observed the conversion of CO to CO_2 by the WGS reaction during the conversion of CH_3OH in syngas over the ZnO−ZrO_2- and ZnO−TiO_2-based bifunctional catalysts (Table S4), whereas no such conversion occurred over the H-MOR−DA+Pt−Sn/SiO_2 catalyst. The WGS reaction was significantly enhanced by addition of ZnO into TiO_2 up to a content of 10 wt %, indicating the role of ZnO in the WGS reaction (Table S4). These experimental facts demonstrate that the removal of H_2O generated during the hydrogenation of AA to C_2H_4 by the WGS reaction on the ZnO-based binary metal oxides is crucial to the stability of the bifunctional catalyst.

Previous studies already clarified that the Brønsted acid sites located in the 8-MR channel of H-MOR account for the AA formation, whereas those in the 12-MR channel are responsible for the formation of hydrocarbons, which eventually lead to coke deposition and catalyst deactivation.[23,25] This insight has rationalized the significant effectiveness of selective removal of Al sites in the 12-MR channel of H-MOR for improving the selectivity of AA and the catalyst stability during CH_3OH carbonylation. On the other hand, the structural requirements for catalytic conversion of AA to C_2H_4 are less understood. In the present work, we discovered for the first time that a new type of hydrogenation catalyst, i.e., the binary ZnO−TiO_2 oxide, shows superior performances for this reaction. Thus, we investigate the structure−performance relationship of the binary metal-oxide-catalyzed hydrogenation of AA.

Structure−Performance Relationships for Acetic Acid Hydrogenation to Ethylene

Transmission electron microscopy (TEM) studies showed that all of the ZnO-based binary metal oxides had the particulate morphology and the ZnO−TiO_2 samples with different ZnO contents had average sizes of around 28 nm (Figures S9 and S10). The specific surface areas of these ZnO−TiO_2 samples were 29−36 $m^2\ g^{-1}$, larger than that of ZnO−ZrO_2 but significantly lower than those of ZnO−SiO_2 and ZnO−Al_2O_3 (Table S5). Thus, the surface area should not be the determining parameter in the hydrogenative conversion of AA. X-ray diffraction (XRD) patterns for ZnO−SiO_2, ZnO−Al_2O_3, and ZnO−ZrO_2 with a ZnO content of 10 wt % only showed diffraction peaks of SiO_2, Al_2O_3, and ZrO_2, respectively

https://doi.org/10.1021/jacsau.3c00463
JACS Au 2023, 3, 2894−2904

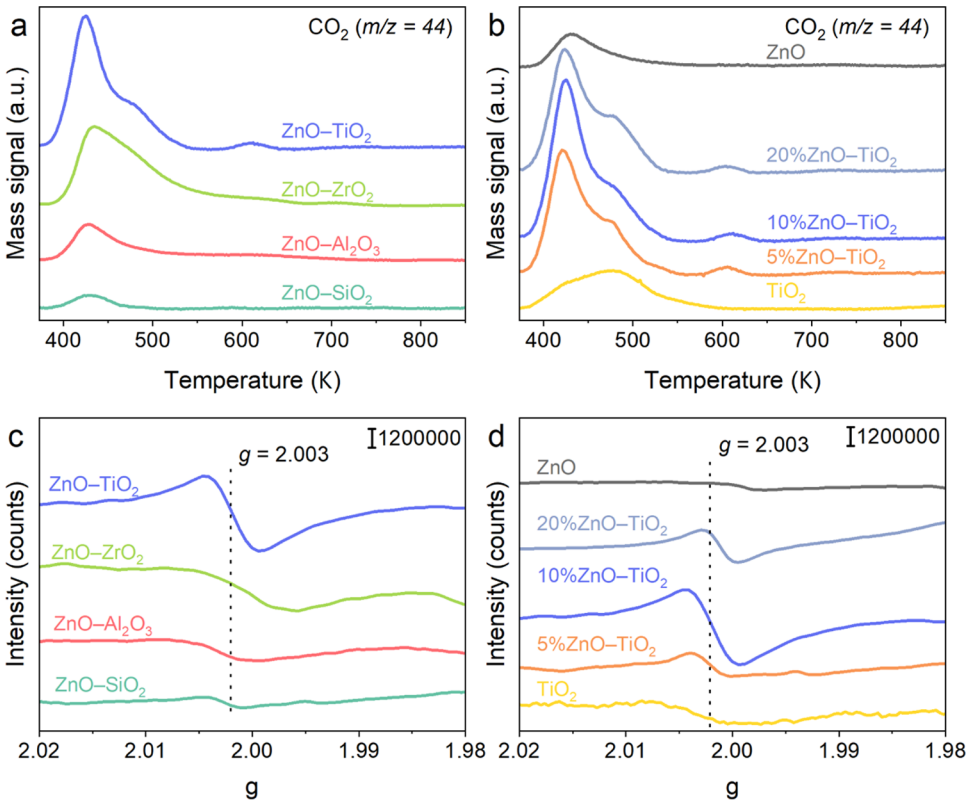

Figure 4. CO_2-TPD and EPR characterization results. (a) CO_2-TPD profiles for different binary metal oxides. (b) CO_2-TPD profiles for ZnO−TiO_2 samples with different ZnO contents. (c) EPR spectra of different binary metal oxides. (d) EPR spectra of ZnO−TiO_2 samples with different ZnO contents.

(Figure S11a), indicating the high dispersion of ZnO in these binary metal oxides. Besides the diffraction peaks of TiO_2, a hexagonal $ZnTiO_3$ phase was clearly observed in the 10 wt % ZnO−TiO_2 and the crystalline ZnO phase was also observed as the ZnO content rose to 20 wt % (Figure S11b). High-resolution TEM (HRTEM) measurements provided further evidence for the presence of $ZnTiO_3$ and ZnO phases in these samples (Figure S12). Small $ZnTiO_3$ domains could even clearly be observed in the 5.0 wt % ZnO−TiO_2, suggesting that ZnO interacted strongly with TiO_2 in the binary ZnO−TiO_2 oxides.

The activation of H_2 would be one determining step for the binary metal-oxide-catalyzed hydrogenation of AA. We performed H_2−D_2 exchange reactions to examine the H_2 activation ability. The normalized HD formation rates were very low on single metal oxides of SiO_2, Al_2O_3, ZrO_2, and TiO_2, and increased significantly by incorporating ZnO into these single oxides (Figure 3a), indicating the role of ZnO in the H_2−D_2 exchange reaction. The incorporation of only 5.0 wt % ZnO into ZnO−TiO_2 could remarkably enhance the HD formation rate and an increase in ZnO content further increased the HD formation rate (Figure 3b). Thus, we propose that the −Zn−O− domain on the binary metal oxide accounts for the activation of H_2. The correlation with the catalytic result that the C_2H_4 selectivity increases with the ZnO content up to 10 wt % (Figure 2b) further demonstrates the role of the −Zn−O− domain in AA hydrogenation to C_2H_4. Although a higher ZnO content of 20 wt % was still beneficial to H_2 activation (Figure 3b), the selectivity of C_2H_4 decreased and that of C_2H_6 increased (Figure 2b), suggesting over-hydrogenation of C_2H_4. Therefore, the content of ZnO in ZnO−TiO_2 is crucial to the selective conversion of CH_3OH to C_2H_4. It is known that H_2 can be heterolytically adsorbed on ZnO surfaces and the formed hydride (H^-) species may participate in the hydrogenation reaction.[29,34,35] Thus, we propose that the hydride species formed on the surface −Zn−O− domain functions for hydrogenation of AA.

The experimental fact that the ZnO−SiO_2 catalyst, which was the least active in AA hydrogenation (Figure 1c), even showed higher H_2−D_2 exchange ability than the ZnO−TiO_2 catalyst (Figure 3a) suggests that there exist other demanding steps besides H_2 activation. We unravel that the adsorption and activation of AA molecules is the other determining step in the hydrogenation of AA to C_2H_4. The FT-IR spectra for the adsorption of AA on ZnO−SiO_2 and ZnO−TiO_2 showed two types of adsorbed species, i.e., the bidentate acetate species (asymmetric stretching at 1575−1535 cm^{-1}, symmetric stretching at 1450−1445 cm^{-1}) and the weakly adsorbed AA molecule (silyl ester C═O at 1750 cm^{-1}, hydrogen-bonded acetic acid molecule with C═O at 1730 cm^{-1} and C−O at 1297 cm^{-1}) (Figure 3c,d).[36,37] These two types of species could be observed over ZnO−SiO_2 at <373 K, but they disappeared at ≥573 K (Figure 3c). In contrast, only the bidentate acetate species were observed over ZnO−TiO_2 and these species could be maintained at ≤673 K (Figure 3d). This clearly demonstrates significantly stronger adsorption of AA on the ZnO−TiO_2 catalyst than that on ZnO−SiO_2. TiO_2 alone displayed similarly stronger adsorption of AA than SiO_2 (Figure S13). Actually, TiO_2 has been widely investigated for the adsorption and conversion of carboxylic acids.[38−41] For the hydrogenation of AA, Pt/TiO_2 was reported to be much more active than Pt/SiO_2, probably due to the unique adsorption

https://doi.org/10.1021/jacsau.3c00463
JACS Au 2023, 3, 2894−2904

property of TiO_2 toward AA.[40] Thus, the unique adsorption behavior of the ZnO−TiO_2 catalyst toward AA should stem from the surface feature of TiO_2.

To gain insight into the active site on metal oxides for the adsorption and activation of AA molecules, we performed the temperature-programmed desorption (TPD) of adsorbed CO_2, a model acidic molecule. Generally, the adsorption of CO_2 takes place either on the weak basic site (including the surface −OH group and the metal−oxygen pair) or on the strong basic site (such as the surface oxygen vacancy) over metal oxide surfaces.[42] The evaluation of the total amount of adsorbed CO_2 by quantification of TPD profiles revealed that the capacity of CO_2 adsorption increased in the order of ZnO−SiO_2 < ZnO−Al_2O_3 < ZnO−ZrO_2 < ZnO−TiO_2 (Figure S14a). The incorporation of ZnO into TiO_2 with a proper content also enhanced the total amount of CO_2 adsorbed (Figure S14b). Moreover, there is no correlation between the amount of CO_2 adsorbed and the specific surface area. Thus, the ZnO−TiO_2 catalyst has intrinsically more abundant active sites for the adsorption of acidic molecules. The in-depth analysis of CO_2-TPD profiles demonstrated that the ZnO−SiO_2 and ZnO−Al_2O_3 catalysts only displayed a low-temperature peak at about 423 K (Figure 4a), and thus, these oxides only had weak basic sites. A shoulder peak at around 483 K was observed for ZnO−ZrO_2 and ZnO−TiO_2, suggesting the existence of basic sites with medium strength on these oxides. A small but distinct peak at around 613 K was further observed for ZnO−TiO_2. This high-temperature peak did not appear for TiO_2 or ZnO alone and became stronger with an increase in the ZnO content from 5.0 to 10 wt % (Figure 4b). These observations suggest the presence of stronger basic sites, probably oxygen vacancy sites, on the ZnO−TiO_2 catalyst surface.

Oxygen vacancies have been proposed to be key active sites for the adsorption and activation of some molecules such as CO, CO_2, and AA on metal oxides.[43−46] The electron paramagnetic resonance (EPR) measurements for our binary metal oxides showed a signal with g value at 2.003 (Figure 4c), which could be assigned to electrons trapped in oxygen vacancies.[30,47] The intensity of this EPR signal increased in the sequence of ZnO−SiO_2 < ZnO−Al_2O_3 < ZnO−ZrO_2 < ZnO−TiO_2 (Figure 4c). The EPR studies further showed that the signal ascribed to oxygen vacancies for ZnO alone was weaker than that for TiO_2, and the incorporation of ZnO into TiO_2 with a content up to 10 wt % further increased the intensity of the EPR signal (Figure 4d). We speculate that the strong interaction between ZnO and TiO_2 may cause a part of low-valent Zn^{2+} to be incorporated into TiO_2 lattice and eventually the formation of $ZnTiO_3$ phase (Figures S11 and S12), resulting in the generation of oxygen vacancies at the same time.[48,49] The correlation of these trends with those obtained from CO_2-TPD and catalytic studies suggests that the oxygen vacancies are responsible for the adsorption and activation of acidic molecules over the metal oxide catalysts, thus contributing to the selective conversion of AA to C_2H_4.

Regarding the mechanism for C_2H_4 formation from AA over the ZnO−TiO_2 catalyst, we speculate that ethanol or adsorbed ethoxyl species may be a key intermediate. Our control experiments using ethanol as a reactant demonstrate that ZnO−TiO_2 is very unique for the selective dehydration of ethanol to C_2H_4. The ZnO−TiO_2 showed not only the highest ethanol conversion but also the highest C_2H_4 selectivity (Table S6). It is of interest to note that the presence of H_2 is required for the selective dehydration of ethanol to C_2H_4 over the ZnO−TiO_2 catalyst (Table S7). Different types of products such as acetaldehyde were formed in the absence of H_2, indicating the occurrence of several different complicated reactions as reported previously.[50,51] The protons derived from the heterolytic activation of H_2 on ZnO−TiO_2 surfaces are proposed to participate in catalyzing the dehydration of ethanol to C_2H_4 in the presence of H_2. These results further demonstrate the unique property of the binary ZnO−TiO_2 oxide in catalyzing the hydrogenative conversion of AA and the synergistic effect of the presence of H_2 in the formation of C_2H_4.

It is noteworthy that although our relay-catalysis route could produce C_2H_4 from CH_3OH with selectivity as high as 85% at complete CH_3OH conversion, which is significantly higher than that in the MTO process, several challenges remain to be solved in the future. First, the separation of C_2H_4 and CO, which is not a concern in the MTO process, should be considered for future larger-scale applications. Second, the high CO/CH_3OH ratio used in the present work causes a low single-pass CO conversion, which is about 3% under typical reaction conditions. This also leads to the need for separation of C_2H_4 and CO and the frequent cycling of CO. A pressure swing adsorption method, which has become a mature technology, may be applied to the separation of CO and C_2H_4.[52,53] Further, the development of more efficient carbonylation catalysts that are capable of working at a low CO/CH_3OH ratio close to stoichiometry (1:1) is needed in the future to increase the single-pass CO conversion and to avoid the C_2H_4/CO separation as well as the frequent cycling of CO.

CONCLUSIONS

We have presented a new relay-catalysis route for the high-selective synthesis of C_2H_4 from CH_3OH in the presence of syngas. A bifunctional catalyst composed of H-MOR−DA and ZnO−TiO_2, which implement CH_3OH carbonylation to AA and AA hydrogenation to C_2H_4 in tandem, offered C_2H_4 selectivity as high as 85% at 100% CH_3OH conversion. Our studies reveal that as a new type of hydrogenation catalyst, the binary ZnO−TiO_2 oxide works uniquely for the selective conversion of AA to C_2H_4. The −Zn−O− domain on the binary metal oxide surface accounts for the activation of H_2, and the surface oxygen vacancies are proposed for the adsorption and activation of AA molecules. Ethanol may be an intermediate in the hydrogenation/dehydration of AA to C_2H_4. The selective removal of Brønsted acid sites via dealumination in the 12-MR channel of H-MOR favors the selectivity of AA in the CH_3OH carbonylation. The *in situ* removal of water formed in AA hydrogenation via the WGS reaction catalyzed by the ZnO−TiO_2 catalyst improves the catalytic stability. We found the synergistic effect of the presence of H_2 in the reactant atmosphere on the product selectivity not only in CH_3OH carbonylation to AA but also in AA hydrogenation to C_2H_4. The present work provides a promising alternative to the MTO reaction for the selective synthesis of C_2H_4 from CH_3OH and demonstrates the usefulness of the relay-catalysis strategy in precise C−C coupling of C1 molecules to C_2 compounds.

https://doi.org/10.1021/jacsau.3c00463
JACS Au 2023, 3, 2894−2904

EXPERIMENTAL SECTION

Materials and Catalyst Preparation

The Na-type mordenite (Na-MOR) with a Si/Al ratio of 6.4 was purchased from Shanghai Fuxu Molecular Sieve Co. H-MOR was prepared by an ion-exchange method. In brief, Na-MOR was dispersed in an aqueous solution of NH_4Cl (1.0 M), and the ion exchange between Na^+ in the zeolite and NH_4^+ in the aqueous solution was performed at 353 K for 4 h under stirring for three times to remove Na^+ thoroughly in the zeolite. H-MOR was obtained after ion exchange, followed by washing with deionized water, drying at 353 K for 12 h, and calcination at 773 K for 5 h. The selective removal of framework Al in the 12-MR channel of H-MOR was performed by a high-temperature steam treatment method reported previously.[21−23,54] The H-MOR sample was first pretreated with pyridine in an Ar atmosphere at 573 K to obtain pyridine-treated H-MOR (Py-H-MOR) with 12-MR channels occupied by pyridine molecules. The obtained Py-H-MOR sample then underwent the ion exchange with an aqueous solution of $NaNO_3$, obtaining a sample containing Na^+ in the 8-MR channel. This sample was calcined at 773 K in air to remove the pyridine molecules in the 12-MR channel. Subsequently, the steam treatment of the obtained sample was performed at 823 K with a gas stream containing 42% H_2O vapor in Ar to remove the Al sites in the 12-MR channel. The presence of Na^+ in the 8-MR channel could sustain most of the Al sites there during the steam treatment. Finally, the sample was subject to the ion exchange with an aqueous solution of NH_4Cl for three times and was calcined at 773 K in air. The obtained sample with a Si/Al ratio of 7.2 was denoted as H-MOR−DA. Other zeolites, including H-SSZ-13 (Si/Al = 13.5), H-ZSM-5 (Si/Al = 100), and H-ZSM-35 (Si/Al = 10.2), were purchased from Nankai University Catalyst Co.

Binary ZnO−TiO_2 oxides with different ZnO contents were prepared by the following procedures. The commercial TiO_2 (P25, 1.0 g) was first immersed in an aqueous solution of $Zn(NO_3)_2$ (concentration, 5.0 mg mL^{-1}). After being ultrasonically treated for 0.5 h, water was removed and the resulting solid was dried at 343 K overnight, followed by calcination at 773 K in air for 6 h to provide ZnO−TiO_2 powders. Other ZnO-containing binary oxides, including ZnO−SiO_2, ZnO−Al_2O_3, and ZnO−ZrO_2, were prepared by the same procedures and the content of ZnO was fixed at 10 wt %. Pt−Sn/SiO_2, an acetic acid hydrogenation catalyst,[23] was prepared by a coimpregnation method. In brief, SiO_2 was impregnated with a mixed aqueous solution of H_2PtCl_6 (concentration, 3.7 mg mL^{-1}) and $SnCl_2$ (concentration, 4.0 mg mL^{-1}), and the loading amounts of Pt and Sn were fixed at 1.0 wt %.

The bifunctional catalyst composed of a zeolite and a metal oxide or Pt−Sn/SiO_2 was prepared by physical mixing of the two components. Typically, the mixture was thoroughly mixed and ground in an agate mortar for 10 min, and the mass ratio of zeolite to metal oxide or Pt−Sn/SiO_2 was fixed at 1:2.

Characterization

XRD patterns were recorded on a Rigaku Ultima IV diffractometer using Cu K_α radiation as the X-ray source. N_2 physisorption measurements were performed on a Micromeritics Tristar II 3020 Surface Area Analyzer. The sample was outgassed in vacuum at 423 K for 4 h before each measurement. Scanning electron microscopy (SEM) measurements were carried out on a Hitachi S-4800 instrument operated at 15 kV. TEM measurements were carried out on a Philips Analytical FEI Tecnai 20 electron microscope operated at an acceleration voltage of 200 kV.

EPR spectroscopy measurements were performed on a Bruker EMX-10/12 instrument at X-band (9.43 GHz, 19.83 mW) incitation and the temperature of samples was controlled at 77 K. The X-ray fluorescence (XRF) analysis was carried out on a Panalytical Axios-Petro XRF instrument with a rhodium target (50 kV and 50 mA). The *in situ* FT-IR measurements were performed on a Nicolet 6700 instrument equipped with an MCT detector. Before measurement, the self-supporting sample wafer was pretreated under vacuum at 773 K for 1 h. Then, FT-IR spectra were recorded from 4000 to 600 cm^{-1} by averaging 64 scans collected at 4 cm^{-1} resolution. For measuring the IR spectra of adsorbed acetic acid, the adsorption was performed at 298 K in an argon gas flow containing 1.0% acetic acid for 0.5 h, followed by evacuation to remove the gaseous acetic acid molecules. The IR spectra of adsorbed species were recorded at different temperatures.

NH_3-TPD measurements were performed on the Micromeritics AutoChem II 2920 instrument. Typically, the sample (0.10 g) was pretreated in a gas flow of He at 673 K for 1 h. Then the adsorption of NH_3 was performed at 373 K in a 10 vol % NH_3−He mixture for 1 h. After removing the gaseous NH_3 or the weakly adsorbed NH_3, the TPD was performed in a gas flow of He by raising the temperature to 1073 K at a rate of 10 K min^{-1}. The signal with m/z of 16 was monitored and recorded online by a mass spectrometer. CO_2-TPD measurements were also performed on the Micromeritics AutoChem II 2920 instrument. Typically, the sample (0.10 g) was prereduced in a 5 vol % H_2−Ar gas flow at 773 K for 1 h. The CO_2 adsorption was performed at 373 K in a 10 vol % CO_2−He gas flow for 1 h, and then the gas flow was switched to He to remove the gaseous CO_2 molecules. The desorption of CO_2 was carried out in the He flow by raising the temperature from 373 to 1173 K at a rate of 10 K min^{-1} and was monitored by a mass spectrometer with the signal of m/z at 44.

The H_2−D_2 exchange reaction was conducted with the following procedure. Typically, the catalyst (0.10 g) was prereduced in the reactor with H_2 at 773 K for 1 h. After the catalyst was cooled down to 583 K, a H_2 gas flow carrying D_2 pulses was introduced into the reactor to perform the H_2−D_2 exchange reaction. The signals of H_2 (m/z = 2), D_2 (m/z = 4), and HD (m/z = 3) in the outlet gas flow were monitored by the mass spectrometer. The normalized HD formation rate was evaluated on the basis of the catalyst weight.

Catalytic Reaction

The catalytic reaction was performed in a high-pressure fixed-bed flow reactor. Typically, the catalyst powders with sizes of 30−60 meshes were loaded in a titanium reactor with an inner diameter of 10 mm and then were prereduced in a 5 vol % H_2−Ar gas flow at 773 K for 1 h. After the reactor was cooled down to 583 K, the reactant gas mixture containing 48 vol % CO, 48 vol % H_2, and 4 vol % Ar was introduced into the reactor and the pressure was raised to 3.0 MPa. CH_3OH was injected into the reactor through a Series III pump. The product was analyzed by an online gas chromatograph equipped with a thermal conductivity detector (TCD) and a flame ionization detector (FID). A TDX-01 packed column was connected to the TCD for the separation and quantification of Ar, CO, CH_4, and CO_2. A RT-Q-BOND-PLOT capillary column was connected to the FID for the separation and quantification of organic compounds. The product selectivity was calculated on a molar carbon basis. The carbon balance was typically better than 95%.

The conversion of methanol in a N_2 or CO atmosphere was performed in the same reactor. The hydrogenation of acetic acid or ethylene was also carried out in the same reactor. Before the experiment, the hydrogenation catalyst was reduced in a 5 vol % H_2−Ar gas flow at 773 K for 1 h. After the reactor was cooled down to 583 K, the acetic acid-saturated vapor (at room temperature) or ethylene was carried by a H_2 stream (H_2/AA = 48/1 or H_2/C_2H_4 = 89/1) into the reactor and the pressure was raised to 3 MPa. The conversion of ethanol in a N_2 or H_2 atmosphere over Pt−Sn/SiO_2 or a metal oxide catalyst was performed after introduction of the liquid ethanol in a N_2 or H_2 atmosphere into the reactor.

The conversion of methanol in syngas with different concentrations of water was performed in the high-pressure fixed-bed flow reactor. The H-MOR−DA was pretreated with a N_2 gas flow at 773 K for 0.5 h. After the reactor was cooled down to 553 K, the methanol solution (with different concentrations of water) was introduced into the reactor using a Series III Pump in the syngas flow at 3 MPa. The water−gas shift (WGS) reaction was conducted in the same reactor. Liquid water was introduced into the reactor using a Series III pump with a CO gas flow.

https://doi.org/10.1021/jacsau.3c00463
JACS Au 2023, 3, 2894−2904

■ ASSOCIATED CONTENT

Supporting Information

The Supporting Information is available free of charge at https://pubs.acs.org/doi/10.1021/jacsau.3c00463.

XRD patterns, SEM micrographs, TEM micrographs, NH_3-TPD, FT-IR spectra, CO_2-TPD, AA-adsorbed FT-IR spectra of metal oxides, and additional catalytic performances for methanol conversion over zeolites or bifunctional catalysts (PDF)

■ AUTHOR INFORMATION

Corresponding Authors

Jincan Kang − *State Key Laboratory of Physical Chemistry of Solid Surfaces, Innovation Laboratory for Sciences and Technologies of Energy Materials of Fujian Province (IKKEM), National Engineering Laboratory for Green Chemical Productions of Alcohols, Ethers and Esters, College of Chemistry and Chemical Engineering, Xiamen University, Xiamen 361005, P. R. China*; orcid.org/0000-0002-0090-8380; Phone: +86-592-2187470; Email: kangjc@xmu.edu.cn

Qinghong Zhang − *State Key Laboratory of Physical Chemistry of Solid Surfaces, Innovation Laboratory for Sciences and Technologies of Energy Materials of Fujian Province (IKKEM), National Engineering Laboratory for Green Chemical Productions of Alcohols, Ethers and Esters, College of Chemistry and Chemical Engineering, Xiamen University, Xiamen 361005, P. R. China*; Phone: +86-592-2187511; Email: zhangqh@xmu.edu.cn

Ye Wang − *State Key Laboratory of Physical Chemistry of Solid Surfaces, Innovation Laboratory for Sciences and Technologies of Energy Materials of Fujian Province (IKKEM), National Engineering Laboratory for Green Chemical Productions of Alcohols, Ethers and Esters, College of Chemistry and Chemical Engineering, Xiamen University, Xiamen 361005, P. R. China*; orcid.org/0000-0003-0764-2279; Phone: +86-592-2186156; Email: wangye@xmu.edu.cn

Authors

Kuo Chen − *State Key Laboratory of Physical Chemistry of Solid Surfaces, Innovation Laboratory for Sciences and Technologies of Energy Materials of Fujian Province (IKKEM), National Engineering Laboratory for Green Chemical Productions of Alcohols, Ethers and Esters, College of Chemistry and Chemical Engineering, Xiamen University, Xiamen 361005, P. R. China*

Fenfang Wang − *State Key Laboratory of Physical Chemistry of Solid Surfaces, Innovation Laboratory for Sciences and Technologies of Energy Materials of Fujian Province (IKKEM), National Engineering Laboratory for Green Chemical Productions of Alcohols, Ethers and Esters, College of Chemistry and Chemical Engineering, Xiamen University, Xiamen 361005, P. R. China*

Yu Wang − *State Key Laboratory of Physical Chemistry of Solid Surfaces, Innovation Laboratory for Sciences and Technologies of Energy Materials of Fujian Province (IKKEM), National Engineering Laboratory for Green Chemical Productions of Alcohols, Ethers and Esters, College of Chemistry and Chemical Engineering, Xiamen University, Xiamen 361005, P. R. China*

Fuyong Zhang − *State Key Laboratory of Physical Chemistry of Solid Surfaces, Innovation Laboratory for Sciences and Technologies of Energy Materials of Fujian Province (IKKEM), National Engineering Laboratory for Green Chemical Productions of Alcohols, Ethers and Esters, College of Chemistry and Chemical Engineering, Xiamen University, Xiamen 361005, P. R. China*

Xinyu Huang − *State Key Laboratory of Physical Chemistry of Solid Surfaces, Innovation Laboratory for Sciences and Technologies of Energy Materials of Fujian Province (IKKEM), National Engineering Laboratory for Green Chemical Productions of Alcohols, Ethers and Esters, College of Chemistry and Chemical Engineering, Xiamen University, Xiamen 361005, P. R. China*

Complete contact information is available at: https://pubs.acs.org/10.1021/jacsau.3c00463

Author Contributions

K.C. and F.W. conducted most of the experiments and analyzed the data. Y.W., F.Z., and X.H. performed a part of catalyst characterizations. J.K. and Q.Z. guided the studies and cowrote the paper. Y.W. supervised the project, designed the study, and cowrote the paper. CRediT: **Kuo Chen** data curation, formal analysis, investigation, validation, writing-original draft, writing-review & editing; **Fenfang Wang** data curation, formal analysis, investigation; **Yu Wang** data curation, formal analysis, investigation; **Fuyong Zhang** data curation, formal analysis, investigation; **Xinyu Huang** data curation, formal analysis, investigation; **Jincan Kang** conceptualization, funding acquisition, methodology, validation, writing-original draft; **Qinghong Zhang** conceptualization, funding acquisition, methodology, writing-original draft, writing-review & editing; **Ye Wang** conceptualization, funding acquisition, methodology, project administration, resources, supervision, validation, writing-review & editing.

Notes

The authors declare no competing financial interest.

■ ACKNOWLEDGMENTS

This work was supported by the National Key Research and Development Program of Ministry of Science and Technology of China (No. 2019YFE0104400), the National Natural Science Foundation of China (Nos. 22121001, U22A20392, 22172123, and 21972116), the SINOPEC Corp, and the Fundamental Research Funds for the Central Universities (No. 20720220008). The authors acknowledge Dr. Yangdong Wang from Shanghai Research Institute of Petrochemical Technology, SINOPEC Corp., for providing helpful discussion.

■ REFERENCES

(1) Olah, G. A. Towards Oil Independence Through Renewable Methanol Chemistry. *Angew. Chem., Int. Ed.* **2013**, *52*, 104−107.

(2) Shih, C. F.; Zhang, T.; Li, J.; Bai, C. Powering the Future with Liquid Sunshine. *Joule* **2018**, *2*, 1925−1949.

(3) Olah, G. A.; Prakash, G. K.; Goeppert, A. Anthropogenic Chemical Carbon Cycle for A Sustainable Future. *J. Am. Chem. Soc.* **2011**, *133*, 12881−12898.

(4) Tian, P.; Wei, Y.; Ye, M.; Liu, Z. Methanol to Olefins (MTO): From Fundamentals to Commercialization. *ACS Catal.* **2015**, *5*, 1922−1938.

(5) Yarulina, I.; Chowdhury, A. D.; Meirer, F.; Weckhuysen, B. M.; Gascon, J. Recent Trends and Fundamental Insights in the Methanol-to-Hydrocarbons Process. *Nat. Catal.* **2018**, *1*, 398−411.

(6) Lin, S.; Zhi, Y.; Chen, W.; Li, H.; Zhang, W.; Lou, C.; Wu, X.; Zeng, S.; Xu, S.; Xiao, J.; Zheng, A.; Wei, Y.; Liu, Z. Molecular Routes of Dynamic Autocatalysis for Methanol-to-Hydrocarbons Reaction. *J. Am. Chem. Soc.* **2021**, *143*, 12038−12052.
(7) Lin, S.; Zhi, Y.; Liu, Z.; Yuan, J.; Liu, W.; Zhang, W.; Xu, Z.; Zheng, A.; Wei, Y.; Liu, Z. Multiscale Dynamical Cross-Talk in Zeolite-Catalyzed Methanol and Dimethyl Ether Conversions. *Natl. Sci. Rev.* **2022**, *9*, No. nwac151.
(8) Wu, X.; Wei, Y.; Liu, Z. Dynamic Catalytic Mechanism of the Methanol-to-Hydrocarbons Reaction over Zeolites. *Acc. Chem. Res.* **2023**, *56*, 2001−2014.
(9) Gao, Y.; Neal, L.; Ding, D.; Wu, W.; Baroi, C.; Gaffney, A. M.; Li, F. Recent Advances in Intensified Ethylene Production−A Review. *ACS Catal.* **2019**, *9*, 8592−8621.
(10) Torres Galvis, H. M.; de Jong, K. P. Catalysts for Production of Lower Olefins from Synthesis Gas: A Review. *ACS Catal.* **2013**, *3*, 2130−2149.
(11) Zhou, W.; Cheng, K.; Kang, J.; Zhou, C.; Subramanian, V.; Zhang, Q.; Wang, Y. New Horizon in C1 Chemistry: Breaking the Selectivity Limitation in Transformation of Syngas and Hydrogenation of CO_2 into Hydrocarbon Chemicals and Fuels. *Chem. Soc. Rev.* **2019**, *48*, 3193−3228.
(12) Pan, X.; Jiao, F.; Miao, D.; Bao, X. Oxide−Zeolite-Based Composite Catalyst Concept That Enables Syngas Chemistry Beyond Fischer−Tropsch Synthesis. *Chem. Rev.* **2021**, *121*, 6588−6609.
(13) Wang, D.; Xie, Z.; Porosoff, M. D.; Chen, J. G. Recent Advances in Carbon Dioxide Hydrogenation to Produce Olefins and Aromatics. *Chem* **2021**, *7*, 2277−2311.
(14) Kang, J. H.; Alshafei, F. H.; Zones, S. I.; Davis, M. E. Cage-Defining Ring: A Molecular Sieve Structural Indicator for Light Olefin Product Distribution from the Methanol-to-Olefins Reaction. *ACS Catal.* **2019**, *9*, 6012−6019.
(15) Zhong, J.; Han, J.; Wei, Y.; Liu, Z. Catalysts and Shape Selective Catalysis in the Methanol-to-Olefin (MTO) Reaction. *J. Catal.* **2021**, *396*, 23−31.
(16) Jiao, F.; Pan, X.; Gong, K.; Chen, Y.; Li, G.; Bao, X. Shape-Selective Zeolites Promote Ethylene Formation from Syngas via a Ketene Intermediate. *Angew. Chem., Int. Ed.* **2018**, *57*, 4692−4696.
(17) Wang, S.; Zhang, L.; Wang, P.; Liu, X.; Chen, Y.; Qin, Z.; Dong, M.; Wang, J.; He, L.; Olsbye, U.; Fan, W. Highly Effective Conversion of CO_2 into Light Olefins Abundant in Ethene. *Chem* **2022**, *8*, 1376−1394.
(18) Haynes, A. Catalytic Methanol Carbonylation. *Adv. Catal.* **2010**, *53*, 1−45.
(19) Cheung, P.; Bhan, A.; Sunley, G. J.; Iglesia, E. Selective Carbonylation of Dimethyl Ether to Methyl Acetate Catalyzed by Acidic Zeolites. *Angew. Chem., Int. Ed.* **2006**, *45*, 1617−1620.
(20) Boronat, M.; Martínez-Sánchez, C.; Law, D.; Corma, A. Enzyme-like Specificity in Zeolites: A Unique Site Position in Mordenite for Selective Carbonylation of Methanol and Dimethyl Ether with CO. *J. Am. Chem. Soc.* **2008**, *130*, 16316−16323.
(21) Zhan, E.; Xiong, Z.; Shen, W. Dimethyl Ether Carbonylation over Zeolites. *J. Energy Chem.* **2019**, *36*, 51−63.
(22) Zhou, W.; Kang, J.; Cheng, K.; He, S.; Shi, J.; Zhou, C.; Zhang, Q.; Chen, J.; Peng, L.; Chen, M.; Wang, Y. Direct Conversion of Syngas into Methyl Acetate, Ethanol, and Ethylene by Relay Catalysis via the Intermediate Dimethyl Ether. *Angew. Chem., Int. Ed.* **2018**, *57*, 12012−12016.
(23) Kang, J.; He, S.; Zhou, W.; Shen, Z.; Li, Y.; Chen, M.; Zhang, Q.; Wang, Y. Single-pass Transformation of Syngas into Ethanol with High Selectivity by Triple Tandem Catalysis. *Nat. Commun.* **2020**, *11*, No. 827.
(24) Blasco, T.; Boronat, M.; Concepcion, P.; Corma, A.; Law, D.; Vidal-Moya, J. A. Carbonylation of Methanol on Metal-acid Zeolites: Evidence for A Mechanism Involving A Multisite Active Center. *Angew. Chem., Int. Ed.* **2007**, *46*, 3938−3941.
(25) Ni, Y.; Shi, L.; Liu, H.; Zhang, W.; Liu, Y.; Zhu, W.; Liu, Z. A Green Route for Methanol Carbonylation. *Catal. Sci. Technol.* **2017**, *7*, 4818−4822.
(26) Cheung, P.; Bhan, A.; Sunley, G.; Law, D.; Iglesia, E. Site Requirements and Elementary Steps in Dimethyl Ether Carbonylation Catalyzed by Acidic Zeolites. *J. Catal.* **2007**, *245*, 110−123.
(27) Xue, H.; Huang, X.; Ditzel, E.; Zhan, E.; Ma, M.; Shen, W. Dimethyl Ether Carbonylation to Methyl Acetate over Nanosized Mordenites. *Ind. Eng. Chem. Res.* **2013**, *52*, 11510−11515.
(28) Cheng, K.; Gu, B.; Liu, X.; Kang, J.; Zhang, Q.; Wang, Y. Direct and Highly Selective Conversion of Synthesis Gas into Lower Olefins: Design of a Bifunctional Catalyst Combining Methanol Synthesis and Carbon−Carbon Coupling. *Angew. Chem., Int. Ed.* **2016**, *55*, 4725−4728.
(29) Liu, X.; Zhou, W.; Yang, Y.; Cheng, K.; Kang, J.; Zhang, L.; Zhang, G.; Min, X.; Zhang, Q.; Wang, Y. Design of Efficient Bifunctional Catalysts for Direct Conversion of Syngas into Lower Olefins via Methanol/Dimethyl Ether Intermediates. *Chem. Sci.* **2018**, *9*, 4708−4718.
(30) Liu, X.; Wang, M.; Yin, H.; Hu, J.; Cheng, K.; Kang, J.; Zhang, Q.; Wang, Y. Tandem Catalysis for Hydrogenation of CO and CO_2 to Lower Olefins with Bifunctional Catalysts Composed of Spinel Oxide and SAPO-34. *ACS Catal.* **2020**, *10*, 8303−8314.
(31) Chen, H.; Cullen, D. A.; Larese, J. Z. Highly Efficient Selective Hydrogenation of Cinnamaldehyde to Cinnamyl Alcohol over Gold Supported on Zinc Oxide Materials. *J. Phys. Chem. C* **2015**, *119*, 28885−28894.
(32) Gliński, M.; Kijeński, J.; Jakubowski, A. Ketones from Monocarboxylic Acids: Catalytic Ketonization over Oxide Systems. *Appl. Catal., A* **1995**, *128*, 209−217.
(33) Rethwisch, D. G.; Dumesic, J. A. Adsorptive and Catalytic Properties of Supported Metal Oxides: III. Water-Gas Shift over Supported Iron and Zinc Oxides. *J. Catal.* **1986**, *101*, 35−42.
(34) Anderson, A. B.; Nichols, J. A. Hydrogen on Zinc Oxide. Theory of Its Heterolytic Adsorption. *J. Am. Chem. Soc.* **1986**, *108*, 4742−4746.
(35) Copéret, C.; Estes, D. P.; Larmier, K.; Searles, K. Isolated Surface Hydrides: Formation, Structure, and Reactivity. *Chem. Rev.* **2016**, *116*, 8463−8505.
(36) Rachmady, W.; Vannice, M. A. Acetic Acid Reduction by H_2 over Supported Pt Catalysts: A DRIFTS and TPD/TPR Study. *J. Catal.* **2002**, *207*, 317−330.
(37) Tackett, J. E. FT-IR Characterization of Metal Acetates in Aqueous Solution. *Appl. Spectrosc.* **1989**, *43*, 483−489.
(38) Thomas, A. G.; Syres, K. L. Adsorption of Organic Molecules on Rutile TiO_2 and Anatase TiO_2 Single Crystal Surfaces. *Chem. Soc. Rev.* **2012**, *41*, 4207−4217.
(39) Lun Pang, C.; Lindsay, R.; Thornton, G. Chemical Reactions on Rutile TiO_2(110). *Chem. Soc. Rev.* **2008**, *37*, 2328−2353.
(40) Rachmady, W.; Vannice, M. A. Acetic Acid Hydrogenation over Supported Platinum Catalysts. *J. Catal.* **2000**, *192*, 322−334.
(41) Lin, F.; Hu, W.; Jaegers, N. R.; Gao, F.; Hu, J. Z.; Wang, H.; Wang, Y. Elucidation of the Roles of Water on the Reactivity of Surface Intermediates in Carboxylic Acid Ketonization on TiO_2. *J. Am. Chem. Soc.* **2023**, *145*, 99−109.
(42) Di Cosimo, J. I.; Díez, V. K.; Xu, M.; Iglesia, E.; Apesteguía, C. R. Structure and Surface and Catalytic Properties of Mg-Al Basic Oxides. *J. Catal.* **1998**, *178*, 499−510.
(43) Polarz, S.; Strunk, J.; Ischenko, V.; van den Berg, M. W. E.; Hinrichsen, O.; Muhler, M.; Driess, M. On the Role of Oxygen Defects in the Catalytic Performance of Zinc Oxide. *Angew. Chem., Int. Ed.* **2006**, *45*, 2965−2969.
(44) Wang, J.; Li, G.; Li, Z.; Tang, C.; Feng, Z.; An, H.; Liu, H.; Liu, T.; Li, C. A Highly Selective and Stable ZnO-ZrO_2 Solid Solution Catalyst for CO_2 Hydrogenation to Methanol. *Sci. Adv.* **2017**, *3*, No. e1701290.
(45) Jia, C.; Fan, W.; Cheng, X.; Zhao, X.; Sun, H.; Li, P.; Lin, N. The Roles of Surface Structure, Oxygen Defects, and Hydration in the Adsorption of CO_2 on Low-Index $ZnGa_2O_4$ Surfaces: A First-Principles Investigation. *Phys. Chem. Chem. Phys.* **2014**, *16*, 7538−7547.

https://doi.org/10.1021/jacsau.3c00463
JACS Au 2023, 3, 2894−2904

(46) Pestman, R.; Koster, R. M.; Pieterse, J. A. Z.; Ponec, V. Reactions of Carboxylic Acids on Oxides: 1. Selective Hydrogenation of Acetic Acid to Acetaldehyde. *J. Catal.* **1997**, *168*, 255−264.
(47) Nakamura, I.; Negishi, N.; Kutsuna, S.; Ihara, T.; Sugihara, S.; Takeuchi, K. Role of Oxygen Vacancy in the Plasma-Treated TiO_2 Photocatalyst with Visible Light Activity for NO Removal. *J. Mol. Catal. A* **2000**, *161*, 205−212.
(48) Kwiatkowski, M.; Chassagnon, R.; Heintz, O.; Geoffroy, N.; Skompska, M.; Bezverkhyy, I. Improvement of Photocatalytic and Photoelectrochemical Activity of ZnO/TiO_2 Core/Shell System through Additional Calcination: Insight into the Mechanism. *Appl. Catal., B* **2017**, *204*, 200−208.
(49) Peng, B.; Tan, L.; Chen, D.; Meng, X.; Tang, F. Programming Surface Morphology of TiO_2 Hollow Spheres and Their Superhydrophilic Films. *ACS Appl. Mater. Interfaces* **2012**, *4*, 96−101.
(50) Rahman, M. M.; Davidson, S. D.; Sun, J.; Wang, Y. Effect of Water on Ethanol Conversion over ZnO. *Top. Catal.* **2016**, *59*, 37−45.
(51) Chagas, L. H.; Zonetti, P. C.; Matheus, C. R. V.; Rabello, C. R. K.; Alves, O. C.; Appel, L. G. The Role of the Oxygen Vacancies in the Synthesis of 1, 3-Butadiene from Ethanol. *ChemCatChem.* **2019**, *11*, 5625−5632.
(52) van Zandvoort, I.; Ras, E.-J.; de Graaf, R.; Krishna, R. Using Transient Breakthrough Experiments for Screening of Adsorbents for Separation of C_2H_4/CO_2 Mixtures. *Sep. Purif. Technol.* **2020**, *241*, No. 116706.
(53) Li, L.; Lin, R.-B.; Krishna, R.; Li, H.; Xiang, S.; Wu, H.; Li, J.; Zhou, W.; Chen, B. Ethane/Ethylene Separation in a Metal-Organic Framework with Iron-Peroxo Sites. *Science* **2018**, *362*, 443−446.
(54) Xue, H.; Huang, X.; Zhan, E.; Ma, M.; Shen, W. Selective Dealumination of Mordenite for Enhancing Its Stability in Dimethyl Ether Carbonylation. *Catal. Commun.* **2013**, *37*, 75−79.

https://doi.org/10.1021/jacsau.3c00463
JACS Au 2023, 3, 2894−2904